NAT'L INST. OF STAND & TECH R.I.C.
A11103 997086
NIST PUBLICATIONS

NISTIR 5170

Measurement Uncertainty Considerations for Coordinate Measuring Machines

S. D. Phillips
B. Borchardt
G. Caskey

U.S. DEPARTMENT OF COMMERCE
Technology Administration
National Institute of Standards
and Technology
Precision Engineering Division
Bldg. 220 Rm. B113
Gaithersburg, MD 20899

QC
100
.U56
#5170
1993

NIST

NISTIR 5170

Measurement Uncertainty Considerations for Coordinate Measuring Machines

S. D. Phillips
B. Borchardt
G. Caskey

U.S. DEPARTMENT OF COMMERCE
Technology Administration
National Institute of Standards
and Technology
Precision Engineering Division
Bldg. 220 Rm. B113
Gaithersburg, MD 20899

April 1993

U.S. DEPARTMENT OF COMMERCE
Ronald H. Brown, Secretary

NATIONAL INSTITUTE OF STANDARDS AND TECHNOLOGY
Raymond G. Kammer, Acting Director

TABLE OF CONTENTS

		page
1	Introduction	1
2	Measurement Uncertainty and Confidence Intervals	2
3	Part Tolerance	3
4	Measurement Uncertainty Due to Part Temperature	8
5	Determining CMM Measurement Uncertainty	10
	5.1 Algorithm Errors	11
	5.2 Operational Errors	12
	5.3 Sampling Strategy Effects	15
	5.4 Measurement Specific Factors	17
6	Empirical Aspects of Determining CMM Measurement Uncertainty	18
7	Interim Testing	20
8	Summary	23
9	Acknowledgments	23
10	References	25
Appendix A		26

Measurement Uncertainty Considerations for Coordinate Measuring Machines

S.D. Phillips, B. Borchardt and G. Caskey
Precision Engineering Division
National Institute of Standards and Technology

Abstract

This report examines some uncertainty considerations for dimensional measurements performed on a three axis coordinate measuring machine (CMM). The interaction between measurement uncertainty and part tolerance is briefly presented, and the factors affecting CMM measurements are discussed and their uncertainty described using the approach recommended by the International Committee for Weights and Measures (CIPM). Several of the current technical difficulties which make a rigorous uncertainty evaluation problematic are considered and some simple examples are presented.

1. Introduction

The use of interchangeable parts, a cornerstone of the industrial revolution, is a result of the capability to produce mechanical parts with sufficiently small variations that they will function equivalently in the final assembly. The concept of interchangeable parts necessitated the invention of part tolerance. The ability to produce parts of sufficiently small variation is based on the ability to measure such small deviations. Consequently, measurement, manufacturing, and tolerance are inextricably linked. Examination of Figure 1 illustrates how the tolerance on precision parts has steadily become more stringent in the past four decades [1,2].

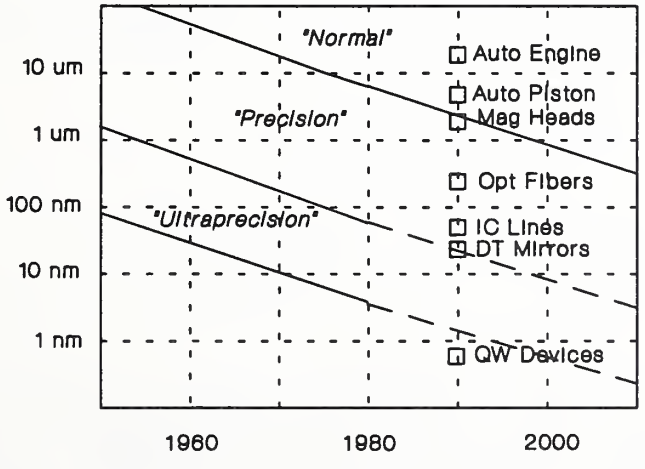

Figure 1. Semilog plot of precision part tolerance vs. year, with examples of state-of-art in 1992.

2. Measurement Uncertainty and Confidence Intervals

In order to sensibly discuss part tolerance we first briefly review the concept of uncertainty using the method recommended by the International Committee for Weights and Measures (CIPM) [3], and being adopted by the International Organization for Standardization (ISO), and by national laboratories including NIST [4,5]. From a quality assurance standpoint, most manufacturers are interested in the fraction of defective parts they are producing, *e.g.* the number of defective parts per million. This implies a confidence interval for the measurand (the specific quantity subject to measurement, such as the length of a part). A confidence interval (of total width $2U_p$) can be expressed mathematically as in equation (1), where y is the result of a measurement, U_p is the expanded measurement uncertainty for the particular level of confidence p (which might be 90%, or 95%, or 99%, etc.), and Y is the measurand (the quantity of interest).

$$y - U_p \leq Y \leq y + U_p \tag{1}$$

We have used the term expanded uncertainty, as recommended by the CIPM, to denote an interval in which the measurement can be expected to lie with a specified level of confidence. Equation (2) describes the connection between the expanded uncertainty at a level of confidence p, and the combined standard uncertainty u_c (which can be thought of as representing one standard deviation of the population resulting from combining all known measurement uncertainties in a root sum of squares - RSS - manner as described later by equation (4)). The coverage factor k_p is a positive real number whose value is selected so that equation (2) is true at a level of confidence p. For example, if u_c is assumed to represent a normal (Gaussian) distribution, then a 99.7% confidence interval in equation (1) corresponds to using an expanded uncertainty obtained with $k_p = 3$ in equation (2).

$$U_p = k_p u_c \tag{2}$$

The combined standard uncertainty u_c can be found by the law of propagation of uncertainty. If the measurand Y depends on N input quantities X_i (i = 1 to N) as shown in equation (3), then the combined uncertainty u_c, of a measurement y, using (best estimated) input quantities x_i, is given by equation (4).

$$Y = f(X_1, X_2, \ldots, X_N) \tag{3}$$

$$u_c^2 = \sum_{i=1}^{N} \left(\frac{\partial f}{\partial x_i} \right)^2 u^2(x_i) \quad + \quad 2 \sum_{i=1}^{N-1} \sum_{j=i+1}^{N} \frac{\partial f}{\partial x_i} \frac{\partial f}{\partial x_j} u(x_i, x_j) \tag{4}$$

The quantities $\partial f/\partial x_i$ are known as the sensitivity coefficients of the measurand with respect to input quantity x_i. The magnitudes of these coefficients describe the importance of the uncertainty associated with each input quantity relative to the total measurement uncertainty. The quantity $u(x_i)$ is the standard uncertainty of the input quantity x_i. This is an estimate of the uncertainty associated with this input variable at the one standard deviation level. The quantity $u(x_i, x_j)$ is the

covariance of x_i and x_j, and is a measure of the correlation between these two input quantities. (If the sources of uncertainty are all uncorrelated then the covariances are zero and the second term of equation (4) can be neglected).

Central to the CIPM method is that all uncertainties are quantified by assigning them a variance (the square root of which is the standard uncertainty, $u(x_i)$, of the input quantity). This includes the usual case of calculating the standard deviation of an input quantity based on a series of repeated measurement using statistical techniques; this is called a type A uncertainty in the CIPM approach. In addition, uncertainties which are not associated with a series of observations are assigned a variance; this is called a type B uncertainty in the CIPM approach. As an example of the latter, the thermal expansion coefficient of a certain type of steel might be stated in a handbook as 11.5 ± 1 ppm/°C. A model of our uncertainty could then be a uniform distribution of total width 2 ppm/°C centered about the 11.5 ppm/°C value. (A uniform distribution is selected because we have no additional knowledge of where the actual value might lie). The standard deviation of a uniform distribution is a well known statistical quantity [3,4]; in the above example $u(\alpha) = 0.58$ ppm/°C.

3. Part Tolerance

Historically, measurement uncertainty has been required to be less than the manufacturing tolerance by a fixed fraction of the tolerance. For example, the "gage maker's rule" calls for a 10:1 [6], (today often employed using 4:1 [7]) ratio of part tolerance to measurement uncertainty. Part tolerance has a well defined meaning as the total amount by which a specific dimension is permitted to vary; the tolerance is the difference between the maximum and minimum limits [8]. Until recently the measurement uncertainty has been assessed using many different methods such as the direct arithmetic addition of errors, root sum of squares (RSS), use of partial derivatives, distribution analysis, or some combination of these or other methods [9]. The use of measurement uncertainty in the gaging ratio method was intended to be applied as a deviation from true value. For example, a part with a dimension stated as ± 20 µm (having a tolerance of 40 µm using the Y14.5 definition) should be inspected by an instrument having a measurement uncertainty of no more than ± 5 µm [10]. Once the gaging ratio rule is satisfied, no further considerations of measurement uncertainty are usually applied to the measurement result, which is taken to be the correct value. Hence, parts are considered functional or nonfunctional based on their "as measured" value. This method has obvious drawbacks as shown in Figure 2 which describes the situation when a 4:1 rule is employed. In Figure 2a the part is considered to be bad (outside the specified tolerance), when in fact it is good (inside the specified tolerance). In this case a good part is rejected. The difference between the true value and the measurement value is the definition of the measurement error, which is small in the case of Figure 2a even though the uncertainty is relatively large. Since the true value is generally unknown, the error is usually unknown; this is one reason the CIPM recommendations regarding measurement results emphasize the uncertainty of the measurement as opposed to its error. Figure 2b illustrates the similar case of accepting a bad part using this "as measured" method of inspection. In Figure 2c the true value lies outside the measurement uncertainty and results in a bad part being accepted. This problem can occur because satisfying a gaging ratio, *e.g.* 4:1, usually does not determine the

confidence of the measurement, *i.e.* the gage maker's rule and confidence intervals are only weakly linked. It may be the case that a specified gaging ratio corresponds to a low confidence, *e.g.* 90%, where the true value of one out of ten measurement results can be expected to lie outside the uncertainty region. Furthermore the gaging ratio method has the unfortunate possibility that whenever a measurement result is close to the tolerance limits, a repeated measurement may yield a different conclusion, *i.e.* a part which is accepted by one measurement may be rejected upon re-measurement.

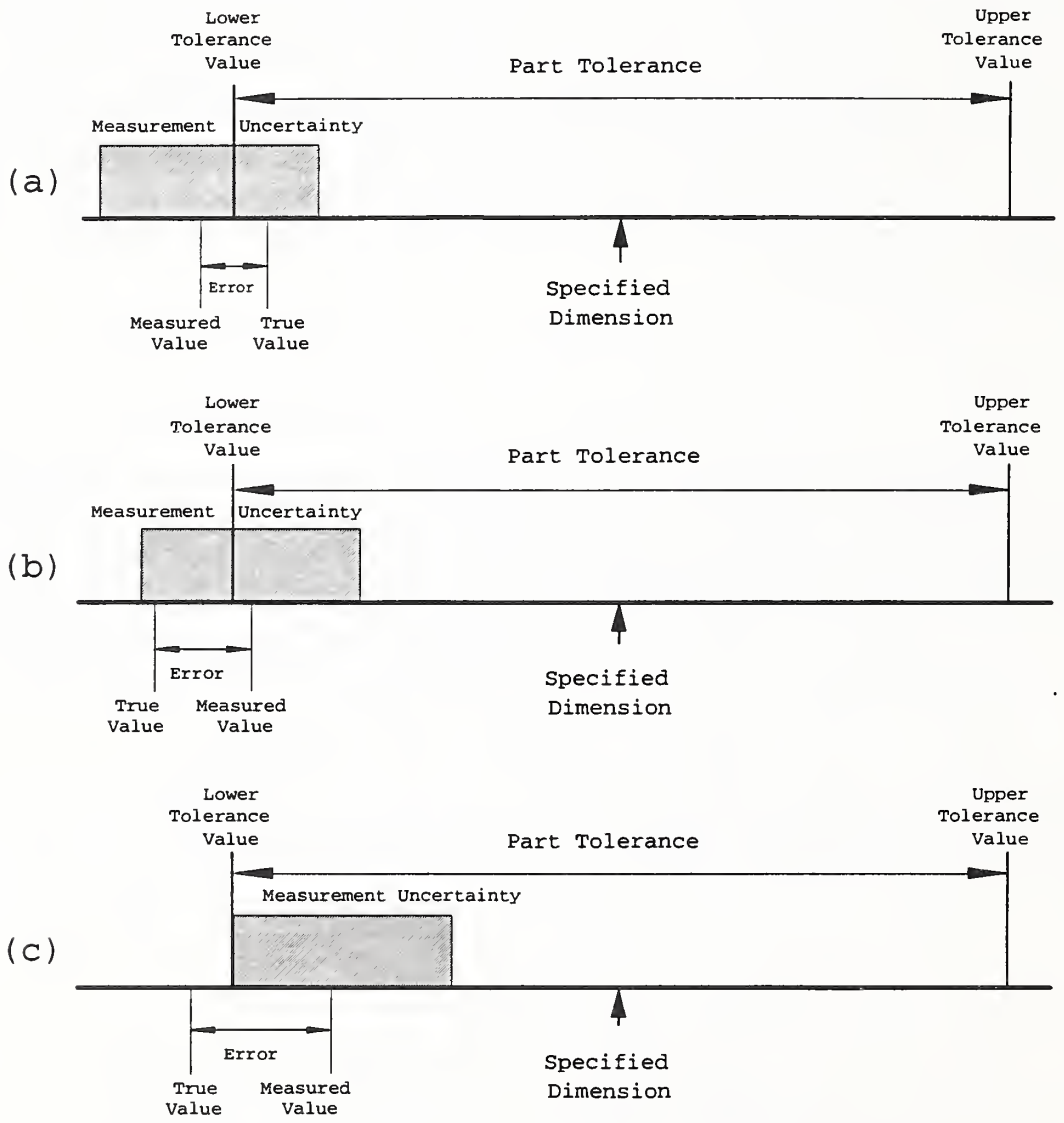

Figure 2: Implications of the gaging ratio method of measurement uncertainty; (a) a good part is rejected due to measurement uncertainty; (b) a bad part is accepted due to measurement uncertainty; (c) a bad part is accepted due to the measurement uncertainty corresponding to a low level of confidence .

Recently it has been suggested [11] to explicitly account for measurement uncertainty when developing part tolerances. This method is sometimes referred to as specifying "guard bands" to protect against measurement uncertainty [12]. In Figure 3 we examine the uncertainties associated with the functional tolerance determination, the customer's inspection ability, and the supplier's inspection ability. (The customer is the person or organization which receives the manufactured part, and the supplier is the person or organization which manufactures the part.) In determining the functional limits of the part, the part designer makes estimates of the deviations from the ideal dimension that can occur and still allow the part to remain functional. This process may involve actual measurements of prototype components, and hence the repeatability and reproducibility of these measurements is important (this is a type A uncertainty). Alternatively, it may involve theoretical calculations which have uncertainties associated with the equation's variables (this is a type B uncertainty). The determination of the combined standard uncertainty, u_c as given by equation (4), takes into account all sources of uncertainties (both type A and B). The part designer determines an expanded uncertainty (see equation (2)) regarding the functional limits based on a level of confidence appropriate to the part; this is denoted by U_f in Figure 3. In order to ensure a functional part at this level of confidence the assigned functional tolerance limit is shifted a distance U_f closer to the ideal specified dimension. The functional expanded uncertainty (U_f) may be different from the customer's expanded uncertainty (U_c) since the part designer may employ calculations or have access to instrumentation not available to the customer who utilizes the part.

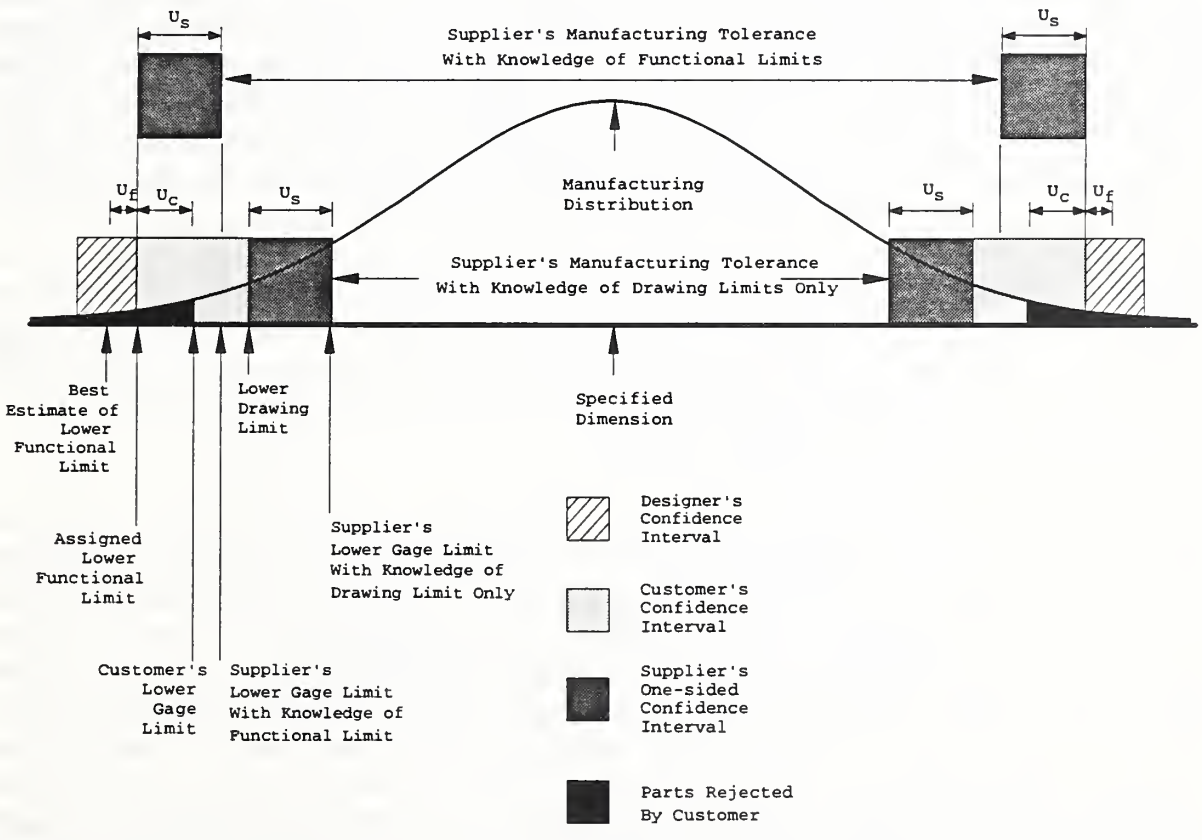

Figure 3 Part tolerance allocation illustrating affects of uncertainties in functional specification, customer's inspection, and supplier's inspection capability.

Based on this tolerance model [11] in which the customer wishes to avoid accepting defective parts (at a level established by his confidence interval), while still being able to prove to the part supplier that a rejected part is out of tolerance (at this level of confidence), the customer will assign the drawing limits by shifting the full width of the confidence interval from the functional limits inward towards the ideal specified dimension, as seen in Figure 3. The drawing limits represent the contractual agreement between the customer and the supplier regarding the part specifications. The customer assigns his measurement gaging limits midway between the functional limits and the drawing limits (assuming a symmetric confidence interval), and rejects parts that are measured beyond this limit, while accepting parts which are measured within this limit. As seen in Figure 3, parts which the customer accepts are functional (at the level of confidence previously determined) even though the true value may fall in the region between the assigned functional limit and the drawing limit (due to measurement uncertainty the exact location of the true value is unknown). Similarly, parts which the customer rejects can be shown (again at the previously determined level of confidence) to fall outside the drawing limits. The true value of some of the rejected parts may be in the region between the assigned functional limit and the drawing limit and hence will function but this cannot be proven due to measurement uncertainty.

If the part supplier has no additional knowledge other than the part drawing limits, then the supplier must set his gaging limits a distance U_s inward from the drawing limits, where U_s is the supplier's expanded uncertainty (set to an appropriate level of confidence). If the supplier has knowledge of the assigned functional limits, then the supplier can set his gaging limits a distance U_s inward from the functional limits which yields a larger manufacturing tolerance zone than in the case where the supplier has no knowledge of the functional limits. There is an obvious economic advantage for the customer to communicate to the supplier the functional limits of the parts since this will allow the supplier to reduce his scrap rate and hence the part price. This benefit must be tempered by the customer's concerns regarding the accuracy and rigor of the supplier's uncertainty evaluation and confidence interval assessment, as this will affect the percentage of incoming parts that the customer decides to inspect. If the customer routinely inspects 100% of the incoming parts then there is no drawback in informing the supplier of the functional limits. Even in this case, the drawing limits still represent the contractual basis of determining if a part is to be accepted or rejected.

Thus far we have not expounded upon how the appropriate confidence interval is selected. Ideally, such a selection is done to economically optimize the entire life cycle of the part including manufacturing, measurement, and use. One necessary factor for this task is the cost function of the part according to the deviation from the ideal dimension. This would include the cost of rejecting a part, and the cost of accepting a bad part, which is usually many times greater than the former. (This is a difficult estimation as it may involve recalling a unit from the field -- or worse yet, involve safety issues.) In addition, any further economic benefit of having a part close to the ideal dimension versus a part within tolerance but borderline (such a borderline part may wear or fail prematurely requiring extra maintenance) should be included in the cost function. To carry out the optimization, estimations of cost as a function of uncertainty are needed for both the measuring and manufacturing distributions. (The standard uncertainty is the

standard deviation of the population, but the shape of the distribution is also required, *e.g.* Gaussian, uniform, etc.)

A thorough optimization will evaluate the economic tradeoffs between different combinations of factors affecting the part over its life cycle. The result will recommend the best combined standard uncertainty u_c (determined by the measuring equipment, strategy, and environment); customer's level of confidence corresponding to U_f (determined by the cost function of the part and of the measurement uncertainty); supplier's level of confidence corresponding to U_s (determined by the supplier's measurement equipment, strategy, environment, and the cost function of the part and of the manufacturing tolerance); whether or not to inform the supplier of the functional tolerance (determined by the part price vs. customer's inspection costs); and the manufacturing process (which determines the shape of the manufacturing distribution and is a result of the production equipment, strategy, and environment).

For precision parts (tight tolerances), the manufacturing costs of part production are usually much larger than the measurement costs. One reason for this is that machine tools must contend with the generation of significant amounts of heat (both from their motors and from the cutting process), large amounts of vibrations, substantial cutting forces, and other factors which degrade their accuracy. Many of these perturbations are absent or reduced in the case of measuring machines; accordingly, for the same level of investment into machine hardware, CMMs are usually much more accurate than their machine tool counterparts. Hence, the increased costs of higher accuracy measurements may be more than offset by the savings resulting from a larger manufacturing tolerance zone yielding a reduced scrap rate. Figure 4 illustrates the economics of CMM measuring capability as assessed by the volumetric performance specification (per ANSI/ASME B89.1.12 [13]), as a function of capital equipment costs for several typical CMMs having approximately one cubic meter of measuring volume.

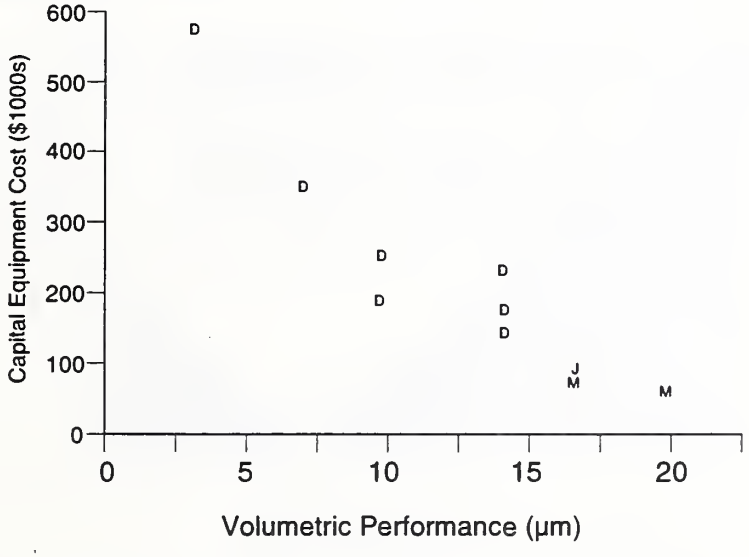

Figure 4 Volumetric performance vs. capital equipment cost for CMMs having approximately one cubic meter of measuring volume; D = direct computer control, J = joy stick, M = manual.

The details of this economic optimization are beyond the scope of this report (further information can be found in reference [12]). Although today most manufacturers do not achieve this level of sophistication in determining manufacturing parameters, it is reasonable to expect that with the advent of inexpensive computing power, such practices will become common due to their significant competitive advantage. In order to carry out such optimizations, detailed models of measurement uncertainty must be developed.

4. Measurement Uncertainty Due to Part Temperature

Ideally the entire measurement process could be mathematically modeled, which would include all relevant parameters which might affect the measurement as indicated in equation (3). A model of the measurement uncertainty could then be developed using the law of the propagation of uncertainty, *i.e.*, equation (4), and the estimation of the variance and covariance of individual uncertainty terms. As a very simple example, consider measuring the distance between two points carried out using a perfect measuring machine on a part whose uncertainty in length is affected only by part temperature. A simple model of the measurement is given by equation (5).

$$L_o = \frac{L_m}{\left(1+\alpha\left(T-T_o\right)\right)} \tag{5}$$

where L_o is the best estimate of the part length after corrections of the measured length (L_m) for all systematic effects; in this simple model the only systematic effect is the expansion of the length due to the part temperature (T) at the time of the measurement, which might be different than the reference temperature (T_o = 20 °C), for a part with thermal expansion coefficient (α).

Following the CIPM recommended procedures for expressing the standard uncertainty u_c for uncorrelated input variables (α and T), yields equation (6), where $\delta\alpha^2$ is the variance characterizing the uncertainty in the thermal expansion coefficient, and δT^2 is the variance characterizing the uncertainty of the temperature measurement. (Note that in this highly simplified example, our perfect measuring machine implies $\delta L_m^2 = 0$; we have also used the fact that $\partial T = \partial(T - T_o)$). Equation (6), which can be evaluated using equation (5) yields equation (7).

$$u_c = \sqrt{\left(\frac{\partial L_o}{\partial \alpha}\right)^2 \delta\alpha^2 + \left(\frac{\partial L_o}{\partial T}\right)^2 \delta T^2} \tag{6}$$

$$u_c = \frac{L_m}{\left(1+\alpha\left(T-T_o\right)\right)^2}\sqrt{\left(T-T_o\right)^2\delta\alpha^2 + \alpha^2\delta T^2} \tag{7}$$

For concreteness we compute the uncertainty of a 1 m long steel part at a variety of temperatures using a coefficient of thermal expansion (CTE) of 11.5 ± 1 ppm/°C (hence $\delta\alpha$ = 0.58 °C), and a temperature sensing system having a combined standard uncertainty of 0.1°C as stated by its manufacturer who used the CIPM uncertainty evaluation method. The CTE of most common engineering materials varies depending upon the specific alloy, the production batch, the heat treatment, and the mechanical history (*e.g.* cold working). Typically the CTE is uncertain at a level of ± 1 ppm/°C [14]. Figure 5 shows both the error due to the (uncorrected) thermal expansion of the part and its associated expanded uncertainty (using a coverage factor of 2 [5]) over the temperature range of 15 °C - 30 °C. Figure 6 depicts only the combined standard uncertainty, which has been separated into the components arising from the uncertainty in the temperature measurement and the uncertainty in the thermal expansion coefficient.

In this example we have assumed that the temperature is uniform and constant throughout the part during the dimensional measurement. In many applications this is not possible because production processes may significantly heat up the part (which may weigh several hundreds or thousands of pounds), and insufficient time is available to allow the part to reach thermal equilibrium. Consequently the part has a non uniform, temporally changing temperature distribution. In particular the surface temperature, due to conduction, convection, and radiative coupling to the environment, may not accurately reflect the internal temperature distribution. If an accurate thermal expansion is required it may be necessary to model the heat flow through the part to determine the temperature distribution, evaluate the material expansion at each different temperature location, and account for stresses and deformations which developed resulting from the non-uniform temperature of the part. Such an exercise would require the use of a finite element analysis computer program, and is beyond the scope of this paper.

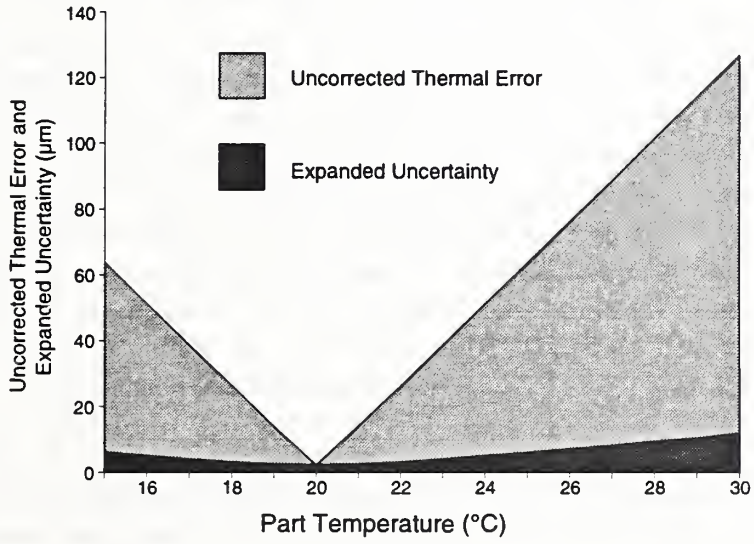

Figure 5 Uncorrected error and expanded uncertainty (k_p = 2) due to the thermal expansion of a 1 m steel part as a function of part temperature (see text for details).

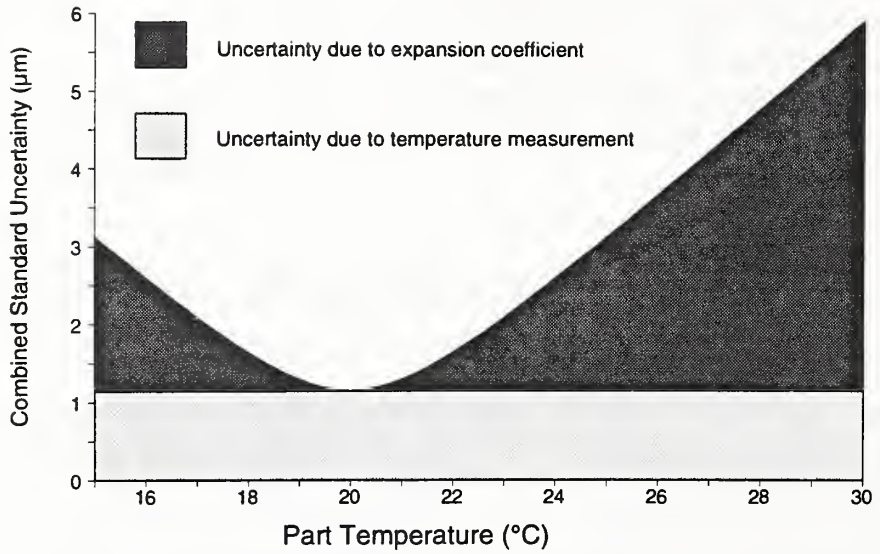

Figure 6 Combined standard uncertainty decomposed into temperature measurement uncertainty and coefficient of thermal expansion uncertainty for a 1 m steel part (using $\delta\alpha = 0.58$ °C and $\delta T = 0.1$ °C).

5. Determining CMM Measurement Uncertainty

Ideally, we would like to be able to write a complete mathematical model of the measurement process, analogous to a very sophisticated version of equation (5), describing all measurements that can be performed on a CMM. Such a model would include all factors which affect the accuracy of the measurement result. By carrying out the law of the propagation of uncertainty (an effort analogous to equation (6) but involving a very large number of variables), a combined standard uncertainty of the CMM measurement could be obtained. (Note that for correlated input variables the propagation of uncertainty must also include the appropriate covariance terms.) Unfortunately, an accurate and detailed mathematical model of CMM measurements is not currently available. Since it is presently not possible to rigorously (a priori) determine the uncertainty for most measurements that a CMM can perform, various national and industrial standards [12,15,16,17] have resorted to characterizing CMM performance through a series of well defined and documented tests conducted on artifacts which are highly idealized (very small form error), and of elementary geometries (circles, spheres, parallel planes, etc.).

Determining the combined standard measurement uncertainty for an actual CMM measurement is a complex task involving several issues. In order to discuss the problem more clearly we distinguish between several different error sources, those of "operational error," "sampling strategy effects," and "algorithm error." (It might be more technically accurate to replace "algorithm error" with "mathematical modeling error," but for the typical CMM user we feel the former may be more familiar.) Figure 7 is a highly simplified block diagram outlining the interaction of these factors in the CMM measurement process.

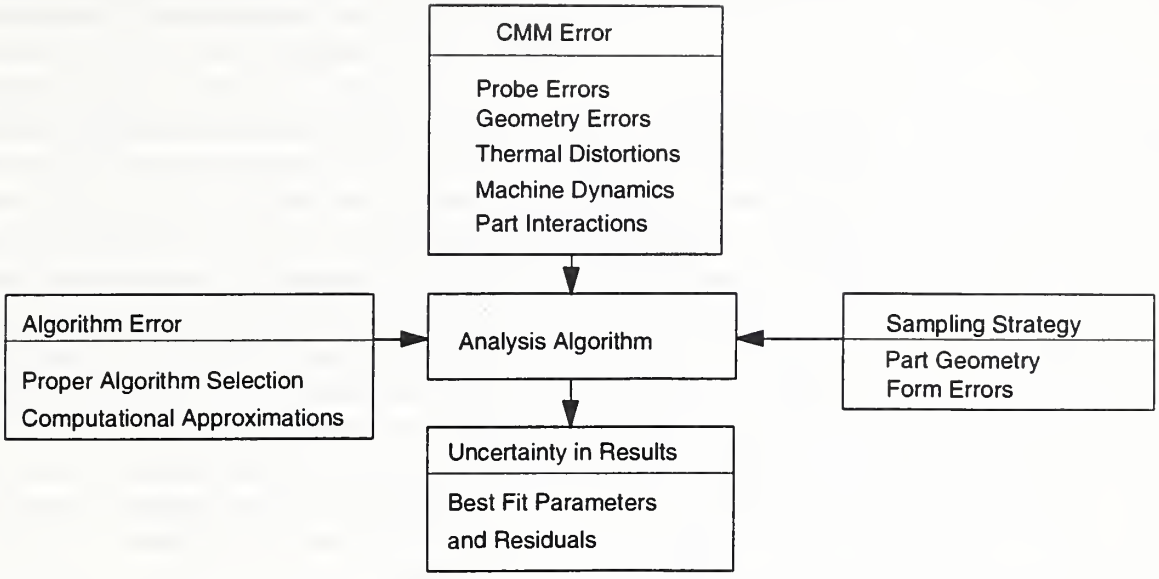

Figure 7 Outline of the sources of uncertainty which affect the computed (best fit) results.

5.1 Algorithm Errors We first consider the algorithm issue. Each part design has a specific intended function which dictates the geometrical dimensioning and tolerancing (GD&T) [8] on the part drawing. The GD&T symbolism specifies a geometrical interpretation which can be assigned a mathematical representation [18]. For a given part feature there may be many different analysis algorithms through which the coordinates of the measured points can be processed. For example, given a nominally circular feature there are several different methods to determine a "diameter" of the feature. These include finding the minimum circumscribed diameter, the maximum inscribed diameter, the minimum zone diameter, the least squares diameter, and a two point diameter (*e.g.* as with a caliper). Even in the case of using a perfect CMM, taking an arbitrarily large number of data points, these different methods may produce significantly different results [19], depending on the details of the part's form error. Hence, even under these ideal conditions a nominally round plug may not physically fit into a hole even though the computed results indicate it should. It should be clear that this "problem" is a result of using the wrong mathematical model in the measurement analysis with regard to the part's intended function. Since most CMMs currently offer only one fitting algorithm (least squares), the calculated solutions may not be indicative of the functional result.

A second issue involves the implementation of the selected algorithm, such as the calculational approximations which are utilized to shorten the time required for computation. For example, many algorithms result in non-linear equations, which are sometimes linearized to greatly speed up the fitting process. Other factors such as finite precision calculations (usually not a problem with modern computers), in addition to outright coding errors, can produce spurious results. Presently, efforts are underway to develop testing procedures to assess the accuracy of CMM analysis software [20]. This is usually carried out by comparison against a reference computer program (which produces the mathematically correct result).

5.2 Operational Errors We define operational errors to include all the uncertainty associated with the measurement instrumentation. This includes the CMM geometrical errors, probe related errors, machine dynamic errors, and errors involving part compensation methods (*e.g.* errors in correcting for the thermal condition of the part as was discussed in section 4 of this paper). Many modern CMMs employ a software error correction program (error mapping) which corrects for the mechanical rigid body errors in the machine. This software accounts for such errors as the pitch, yaw, roll, straightness, and scale errors of each machine axes (as a function of the axis position), and the three squareness errors between the axes. These errors are an inevitable result of the CMM manufacturing and assembly process, and error mapping can compensate for the majority of the CMM's rigid body errors. However, since the error mapping process also has some uncertainty associated with it, there are some small residual rigid body errors remaining. The distribution of these residual errors is dependent upon the error mapping coordinate system, whereas the correction itself is independent of the mapping coordinate system. This occurs because the mapping technique makes use of a set of lines which are defined to have only translational errors, with the angular errors defined to have their centers of rotation on these lines. Consequently, for a typical error mapped CMM the measurement uncertainty increases in magnitude with distance from these lines making the residual error distribution dependent on the mapping coordinate system. We note that such residual errors are also present in even the most mechanically accurate CMMs since either method of error correction (in software or in hardware, *e.g.* by scraping the axis ways) requires dimensional measurements which introduce measurement uncertainty. (A mechanically corrected CMM may also provide corrections for other errors in addition to rigid body effects.)

Non-rigid body behavior is another source of CMM error arising from structural deformations produced by such sources as over constrained mechanical systems, *e.g.* table bending on some moving table CMMs, deformations due to part loading, and deformations due to self loading, *e.g.* ram bending on horizontal arm moving ram CMMs. Some of these deformations are naturally included in a rigid body error map, *e.g.* the deformation of a CMM bridge as the ram carriage moves across it appears as a straightness error in a rigid body error map. In principle elastic deformations can be error mapped although this is a more complex problem than the simple rigid body case. In any event, non-rigid body behavior introduces errors into the CMM coordinate system which must be accounted for in an uncertainty analysis.

One major error source is due to structural deformations caused by the thermal condition of the CMM. Most CMMs are specified to operate over a narrow range of thermal conditions; however, in practice they are often used well outside these limits. The simplest part of this problem is the uniform expansion of the CMM scales and of the part, which can be easily treated by a linear correction as described in section 4 of this paper. A much more difficult issue is the actual geometrical distortions of the CMM structure (and the part as discussed in section 4), which is highly specific to the details of the CMM design and the exact temperature distribution throughout its structure. We point out that thermal gradients can develop even when the CMM is in a homogenous temperature environment, if the entire environment is changing in time. This is a result of the different thermal time constants of the various components of the CMM. It is widely recognized that thermal effects degrade CMM accuracy and a crude estimate of this problem has been developed using the thermal error index method which amounts to a thermal

drift test and an estimate of the uncertainty in the linear coefficient of thermal expansion [13]. Unfortunately, little detailed knowledge is presently known about the nature of these thermal errors and their resultant impact on CMM measurements

Several error sources depend on the specifics of the measurement plan. For example machine dynamic errors depend on such factors as probing speed, probing direction, probe approach distance, acceleration values, etc. Figure 8 illustrates a dynamic error (primarily due to machine structure oscillations) which is highly dependent on the probe approach distance. This figure shows the variation in apparent position of a gaging surface as a function of probe approach distance for a constant probe approach velocity of 8 mm/s. At large distances the oscillations are damped out prior to the probe triggering. This effect is highly repeatable, so if the CMM probe is calibrated and used at the same probe approach distance this dynamic error can largely be accounted for. However, if the user changes the probe approach distance (without requalifying the probe) then significant errors could be introduced into the measurement. (This might induce a shift from a peak to a valley in Figure 8.)

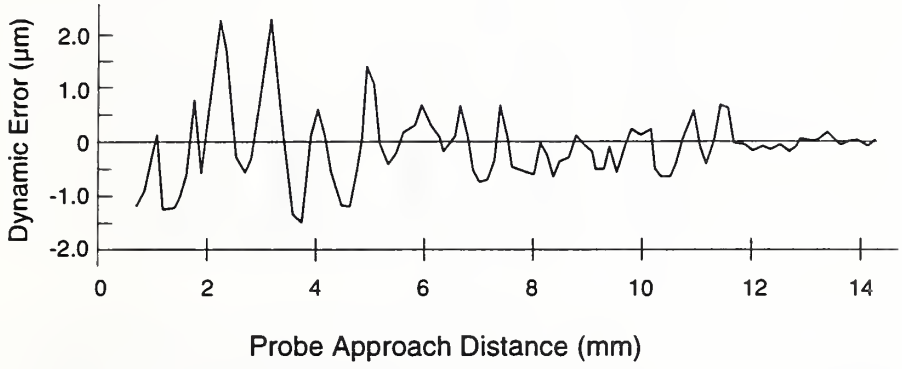

Figure 8 Apparent distance variations due to CMM dynamics as a function of probe approach distance.

The CMM probe may also be a source of measurement uncertainty. Many touch trigger probes in common use today have direction dependent errors. These probes require a small amount of deflection before the probe triggers; this amount of deflection is known as the pretravel. The amount of pretravel is dependent on the direction of deflection, and is referred to as pretravel variation. When a probe, (stylus) is calibrated the effective stylus ball diameter is assigned a value which accounts for the average amount of pretravel (strictly speaking this is usually a least squares fit of the different pretravel values encountered during the stylus calibration). One aspect of pretravel variation is easily seen by measuring a ring gage as shown in Figure 9. The ring gage (which is round at a level of 0.1 µm), typically appears as having three lobes (which is a result of the kinematic stylus mount located inside the probe). The magnitude of the pretravel variation is dependent on the stylus length as shown in the figure. This effect is also dependent upon the orientation of the probe. When the probe is vertical, as when measuring a ring gage in the plane of the table, gravity has little effect on the pretravel variation. When the probe and stylus are oriented horizontally, as when measuring a ring gage mounted perpendicular to the table, gravity

pulls on the stylus changing the pretravel variation. This is most apparent for the largest (100 mm) stylus.

Another method to quantify probe pretravel variation, *i.e.* probe lobing, is defined in the ANSI standard [13]. This method, called the point-to-point performance test, involves taking 49 points on a nearly perfect sphere, each at a different position on the sphere's surface (this covers an entire hemisphere plus some points slightly below the equator). The range of measured radii from the best fit center to each of the 49 points is taken as the probe performance value. We have carried out this test for a typical touch trigger probe using both a 10 mm and 50 mm stylus, as shown in Figure 10.

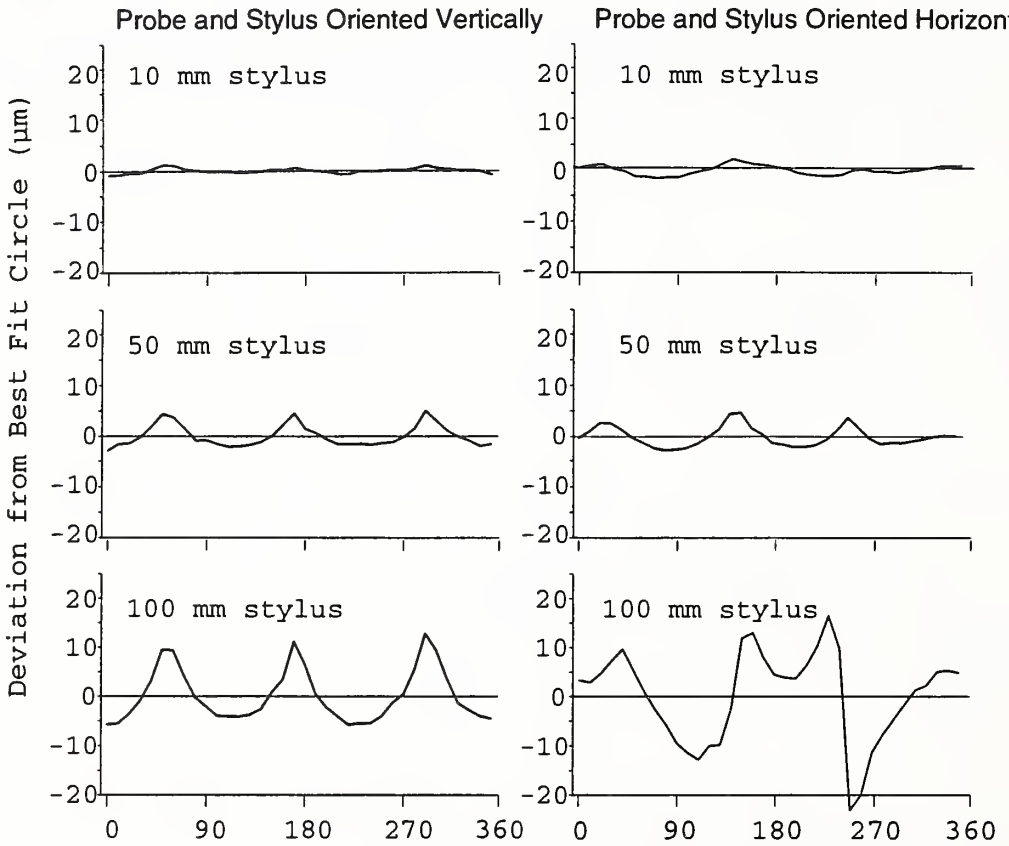

Figure 9 CMM probe pretravel variation as measured using a ring gage for three different stylus lengths. Left, probe and stylus are oriented vertically, measuring a ring gage mounted in the plane of the table. Right, probe and stylus oriented horizontally, measuring a ring gage mounted perpendicular to the plane of the table.

It is interesting to compare the results of the normal point-to-point performance test to that obtained when using a number of different styli or probe head positions. Many CMM measurements involve using either multiple styli (as with a star probe), or multiple probe orientations (as with an indexable probe head). When these different styli or probe orientations are utilized in a single measurement it is very important to know the position of each stylus ball relative to the other positions. The location of the stylus ball relative to the end of the CMM ram

is known as the probe offset vector. Errors in the offset vectors become measurement errors when multiple styli or probe positions are used in a measurement. Figure 10 includes a 49 point probe performance test which was taken using eight different probe head positions. (Six points were taken in each of seven probe head positions and seven points were taken in the eighth position.) The significantly larger performance test values when using multiple probe positions versus using only one position is due to several different factors. These include the errors in the effective stylus ball diameter, errors in the probe offset vectors, and probe head repeatability problems. These errors must be assessed and accounted for when evaluating CMM measurement uncertainty when using multiple styli or probe positions in a single measurement.

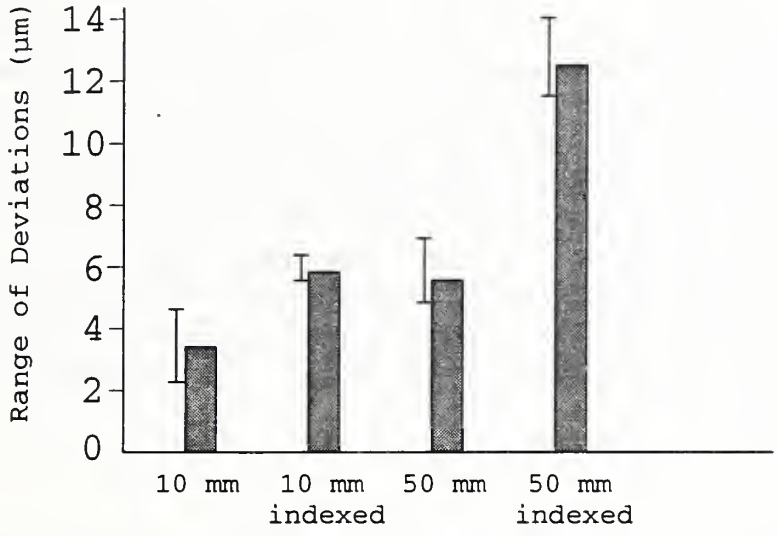

Figure 10 The point-to-point probe performance test results from using 10 mm and 50 mm long styli. The results show both the standard single probe position case and the multiple probe position case where the probe was indexed through eight different positions. The solid bars represent the mean of five test results, and the adjacent lines show the range of five tests.

5.3 Sampling Strategy Effects The effect of selecting a measurement sampling strategy has recently been recognized as a major component of measurement uncertainty [19,21]. By sampling strategy we mean the number and position (relative to each other) of the sampled points on the part surface. Since most CMM measurements today use a relatively few number of points (typically less than ten per part feature) to determine the part geometry (this calculated geometry is often called the substitute geometry), it must be recognized that the computed result amounts to an extrapolation based on incomplete part information. For example, consider a perfect CMM, in a perfect environment, using a perfect algorithm, which measures a part having some (unknown) form error. If the part is now remeasured using a different sampling strategy (or the same sampling strategy with the points taken at different positions on the part) a different result will be computed. In this example each measurement result is "correct" given the limited information provided by the small number of measured points. The variation in the results is a consequence of different (and incomplete) part information being supplied to the algorithm in

each case. Some sampling strategies can greatly amplify the error introduced at each measurement point, while other sampling strategies can reduce this error. If the part was measured using an infinite (or very large) number of points, then regardless of the nature of the form error or the part orientation upon remeasurement (using a perfect measuring system) the same answer would be obtained in all cases. The difference in the computed results between the finite and infinite sampling case is the error due to the finite sampling strategy. Since it may not be practical to measure a large number of points for each feature, this sampling strategy effect must be accounted for when determining the combined standard uncertainty of a CMM measurement.

Figure 11 illustrates the effect that the sampling strategy has on a least squares algorithm determining the best fit center location for a circle. The figure depicts a circular feature having an elliptical form error (which has been greatly amplified for clarity) of 10 μm out of roundness, which is measured with three different sampling strategies. If the part is randomly rotated with respect to the sampling strategy a different center location may be calculated. Randomly rotating the part a large number of times creates a distribution of center locations as shown in Figure 11. We note that Figure 11(d) is a special case of a more general theorem regarding least squares fitting algorithms for circles or spheres: If a circle (or sphere) possesses a form error which has inversion symmetry through its center, and if this circle (or sphere) is measured using a sampling strategy which has inversion symmetry then the least squares best fit center location will be the correct (infinite sampling case) center, regardless of the relative orientation of the form error to the sampling strategy [22].

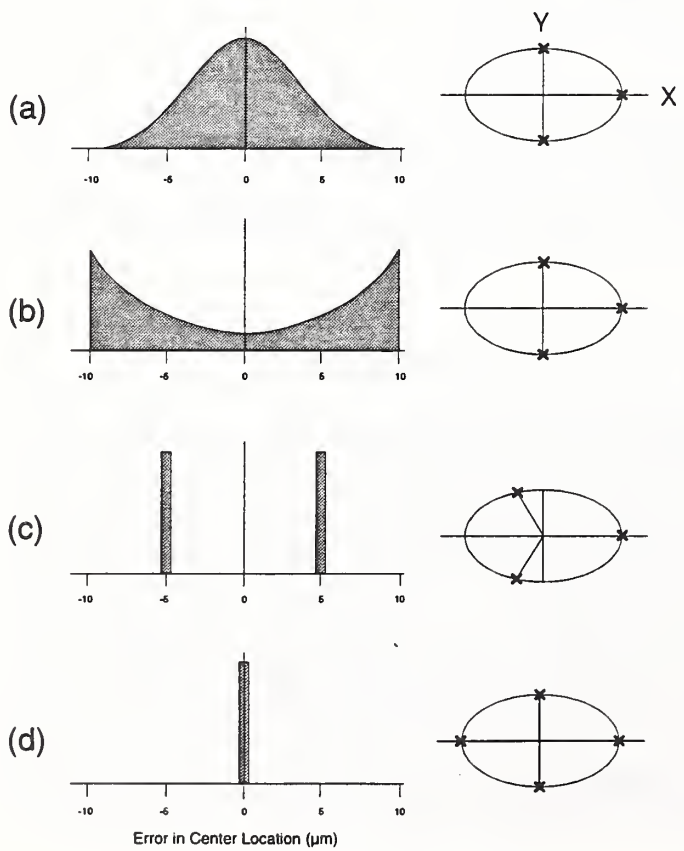

Figure 11
Distribution of distances between the best fit center location and the true center position (given by the infinite number of sampling points case) for a circle having a 10 μm elliptical form error. (For clarity we define the sign of the distance to be that of the X coordinate of the computed center.) (a) a naive and incorrect guess of a normal distribution for a three point (90° spaced) sampling strategy; (b) the correct distribution for a three point (90° spaced) sampling strategy; (c) a three point (120° spaced) sampling strategy (note that the correct center is never found); (d) a four point (90° spaced) sampling strategy which always locates the correct center.

5.4 Measurement Specific Factors Although Figure 7 gives an overview of the measurement process, it tends to falsely imply a static nature to the measurement errors. When a user performs a CMM measurement, several factors simultaneously interact. First the user determines the type of measurement to perform; this fixes the algorithm for both the geometry (circle, sphere, etc.) and the calculational type (min-max, least squares etc.). Secondly, the user determines the sampling strategy, *i.e.,* the number and location of points to be measured. The selected sampling strategy determines where (and how) the CMM must move to take measurements. This establishes what CMM errors occur and which aspects of the part's form error are measured. These factors have important implications to the stability and accuracy of the computed (best fit) results.

We note that a CMM is often thought of as having an error vector attached to each point in space within the measuring volume representing the sum of all the imperfections in the CMM. A more realistic paradigm is to view each point in the measuring volume as having an "uncertainty cloud" associated with it. The size and shape of this cloud is determined by the error sources of the CMM. When a probing point is measured a particular error vector is "precipitated" out of the cloud. This error vector is the difference between the coordinates the CMM records at a measurement point and the true coordinates in a perfect coordinate system. If a different measurement is performed at the same point a different error vector will usually result. This occurs because the error depends on many measurement specific factors, such as the probe approach direction, the probe approach velocity, interactions between the probe and the part surface etc., as well as the particular state of the CMM's geometrical structure (which is usually changing with time because of thermal perturbations from the environment). Hence, the measurement error vector is not determined until the user actually performs the measurement. (Unlike the quantum mechanical situation, this classical system has hidden variables, such as the exact nature of the thermal distortions at the time of measurement; however these details are difficult to predict.) The implications of the user involvement are more clearly stated in Figure 12 which provides a more detailed outline of the measurement process.

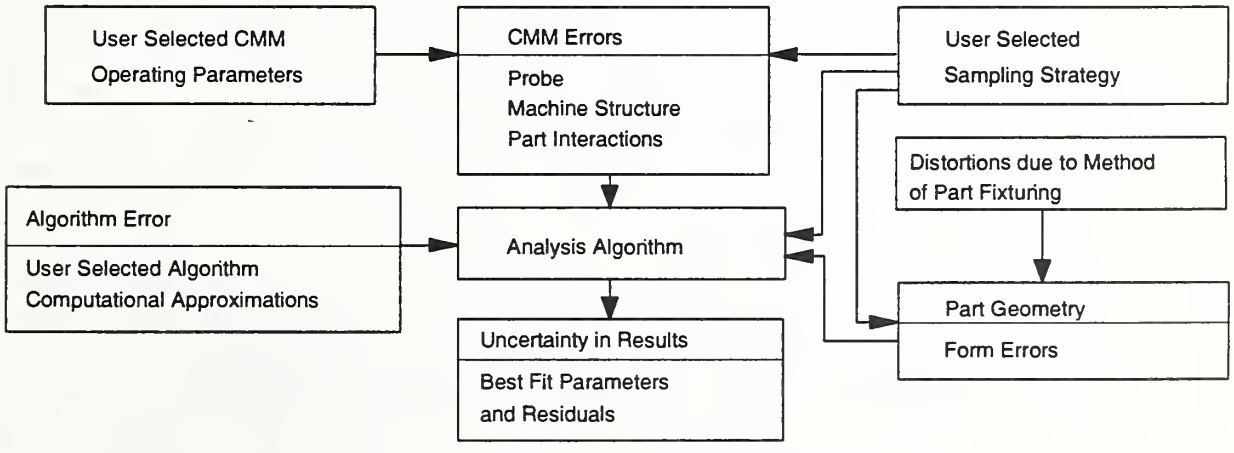

Figure 12 Schematic of the sources of uncertainty which affect the computed (best fit) results with emphasis showing the influence of the CMM user.

6. Empirical Aspects of Determining CMM Measurement Uncertainty

Since a rigorous mathematical methodology is currently unavailable, we might hope to develop a semi-empirical model of the measurement process. A measurement can be thought of as probing n points on the part's surface, this is given by the vector $\mathbf{r}_i$ in Figure 13 (where the subscript denotes the ith point in the n point set). The number and location of these points is determined by the sampling strategy. Each of these points can be decomposed into two vectors $\mathbf{R}_i$ and $\mathbf{E}_i$ as shown in the figure. $\mathbf{R}_i$ represents the (ith) point coordinate vector which would have been obtained in a perfect measurement system (note that this includes the form error of the part caused by imperfect manufacturing), and $\mathbf{E}_i$ represents the error introduced by the actual measurement system. The vector $\mathbf{E}_i$ includes errors from the CMM structure, the probe, and those introduced into the part during the measurement process (such as distortions arising from imperfect fixturing and from the environment). This error vector can be thought of as resulting from the uncertainty in the true point coordinate $\mathbf{R}_i$. In evaluating CMM measurement uncertainty, the magnitude of $\mathbf{E}_i$ must be determined, *i.e.* the variance of this input quantity using the CIPM terminology. The effect that this uncertainty has upon the computed results (the sensitivity coefficient) is determined by examining the variations of the (best fit) results relative to variations of the input quantity. Depending on the sampling strategy, the same error vector can have very different effects on the computed results, *i.e.* the sensitivity coefficients are highly dependent on the sampling strategy (and also on the type of algorithm) [19,22]. Consequently, for each common sampling strategy (*e.g.* six equally spaced points), for each type of measurement geometry (circle, plane, etc.), for each type of algorithm (least square, min-max, etc.), we must determine the sensitivity coefficient. Once this effort is completed the results can be used for all future CMM measurements, as the sensitivity coefficients are not CMM specific.

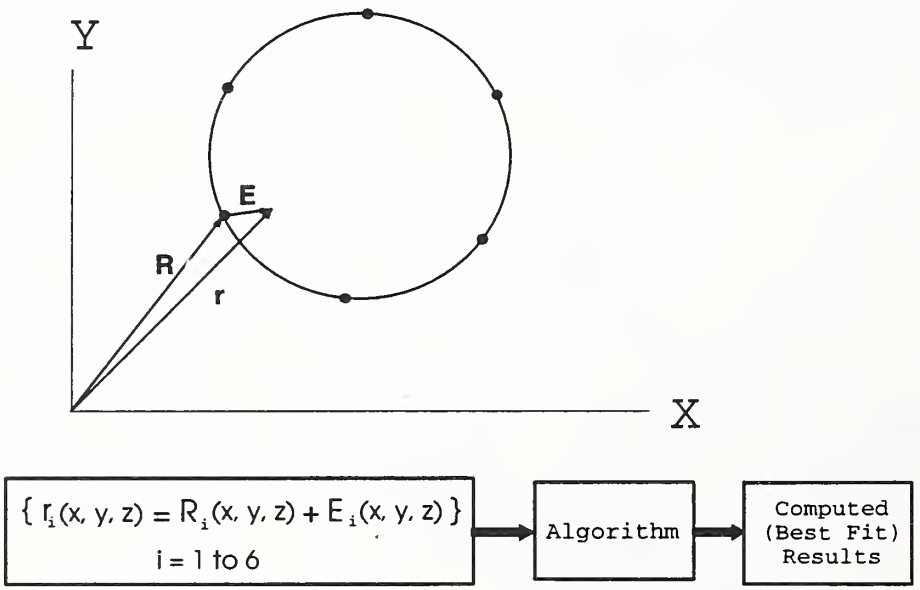

Figure 13 Measuring a circular feature using six equally spaced points; **R** is the true point coordinate vector which would be found using a perfect measurement system; **E** is the

error vector introduced in the actual measurement; **r** is the resulting point coordinate vector measured by the CMM.

The actual magnitude of $\mathbf{E}_i$ is highly specific to each CMM, its environment, and its user. Presently, lacking a detailed model of CMM behavior, these errors need to be experimentally determined. Appendix A is a first effort at identifying variables which affect CMM measurements; several of these error sources have already been discussed. Many of these factors are interdependent or correlated, making it difficult to account for their effects independently. Consequently, care must be taken not to overcount each effect when empirically considering their contributions to the combined standard uncertainty. The degree to which different effects are separated or combined is determined by the level of accuracy needed and the degree to which it is possible to separate these effects.

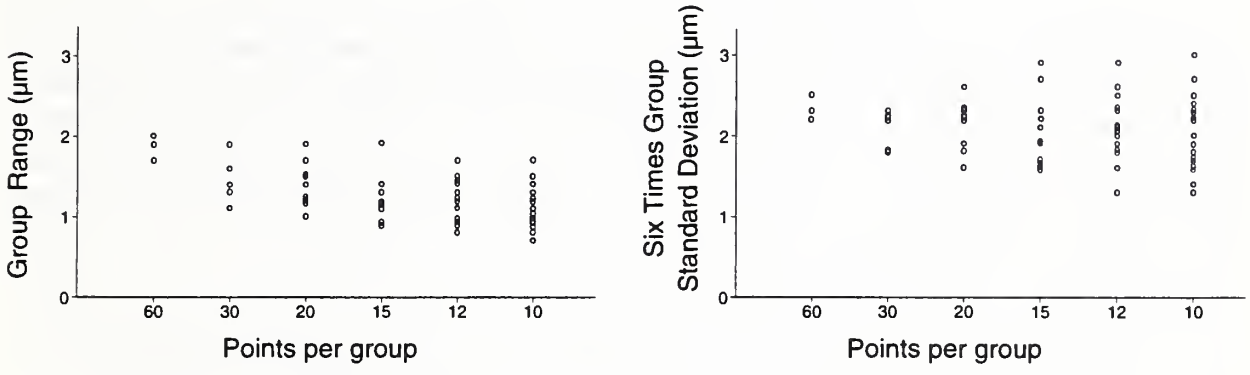

Figure 14 The range of center coordinates of 180 sphere fits arranged in groups of size varying from 10 to 60 sphere coordinates per group (left). The same data analyzed in a similar manner using the group standard deviation (right).

Typically it is easier to assess some quantities such as probe and CMM repeatability as a combined error instead of independent quantities. For the case of repeatability this is a useful approach since the probe and CMM are used together as a unit, and it avoids the problem of how to combine the two uncertainties. In order to have a reasonable assessment of an input quantity it is necessary to have enough measurements to produce a statistically stable value. As an example, consider the ANSI definition of CMM repeatability, which is operationally defined as the range in the measured coordinates of ten sphere centers, each found using four probing points [13]. To test the stability of this parameter, we measured a sphere 60 times (each with four points) at three different locations in the measuring volume of a moving bridge CMM for a total of 180 sphere measurements (the different locations allow us to determine if the repeatability is position dependent). Each set of 60 sphere centers was separated into 6 groups of 10 measurements (the ANSI specified quantity), and the range of that group computed and displayed in Figure 14. As seen in the figure these 18 groups (3 x 6) differ widely (from 0.7 µm to 1.7 µm), and hence the repeatability parameter as defined is not very stable. By using the same data but rearranging the number of sphere centers into groups of 12, 15, 20, 30, and 60 we obtain the data shown in Figure 14. It is clear that a group size of 60 or more sphere measurements is needed before stable

test results are reached, which occurs at the 2 μm level in the figure (this is well within the 3 μm value specified for this CMM). We note in passing that the ANSI standard was designed to provide CMM specifications between a CMM vendors and customers, and not necessarily to provide stable test procedures for the user. Also shown in the figure is the standard deviation results for the same data which is of more interest in the CIPM uncertainty approach. Since the three groups of 60 results, each taken at a different position within the CMM volume, appear to be converging to a common value this is a good indication that the repeatability is not position dependent. Unfortunately, a complete set of tests needed to identify and quantify all the various input (error) quantities has not been established.

7 Interim Testing

Once a CMM has been calibrated (establishing the measurement uncertainty), it is prudent to periodically check to see if the calibration is still valid. Such an interim test should include as many components of the measurement system as possible. The frequency and extensiveness of the test should be determined by the user, appropriate to the type of the measurements the CMM is used for. We describe one simple test below which is appropriate for a CMM with an approximately cubical work zone. This test employs a ball bar which has been calibrated for ball form (roundness), ball size (diameter), and center to center length. With the ball bar placed along a body diagonal (see Figure 15), each sphere is measured using many, *e.g.* 6 - 10, points. Since the balls are easily accessible from a number of different directions, multiple stylus tips (of a stylus tree), or multiple probe positions (on an indexable probe head) can be used to measure the points on each sphere, if such accessories are a part of the normal operation of the CMM. If a probe (or stylus) changer is available, probes (or styli) can be swapped when measuring the points on the sphere to include the probe changer in the interim test. This procedure is carried out for each of the four body diagonals of the work zone, as shown in Figure 15. These positions are chosen because they are sensitive to common problems.

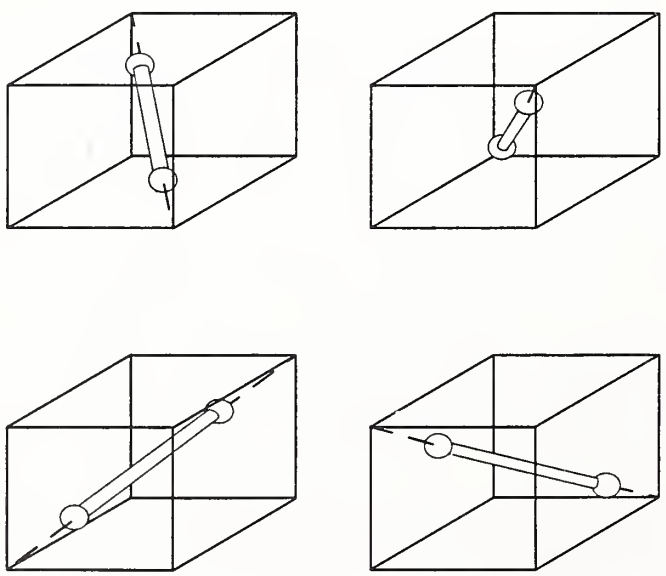

Figure 15 Ball bar positioned for an interim test along the four body diagonals in a roughly cubic CMM work zone.

Figure 16 illustrates a typical result of the previously described interim test, using eight probing points on each sphere. We have plotted the difference between the best fit radius and the radii to each of the eight probing points taken from the best fit center. Since a total of eight spheres are measured during the test (two per ball bar position, and four ball bar positions) the figure shows eight groups of eight radial differences each. We have also plotted the difference between the best fit sphere diameter and its calibrated value. Also shown in the figure are the four center to center bar lengths.

Employing a ball bar in this test has several advantages. When probing the spheres the exact location of the probing points are unimportant (provided they do not all fall into a plane) since there are no preferential locations on the sphere's surface, as opposed to measuring a gage block where care is required to avoid an alignment (cosine) error. Since precision spheres are widely available and the exact physical length of the complete ball bar assembly is unimportant (the exact ball bar length and ball size are determined by its calibration), the ball bar is an inexpensive and readily available artifact.

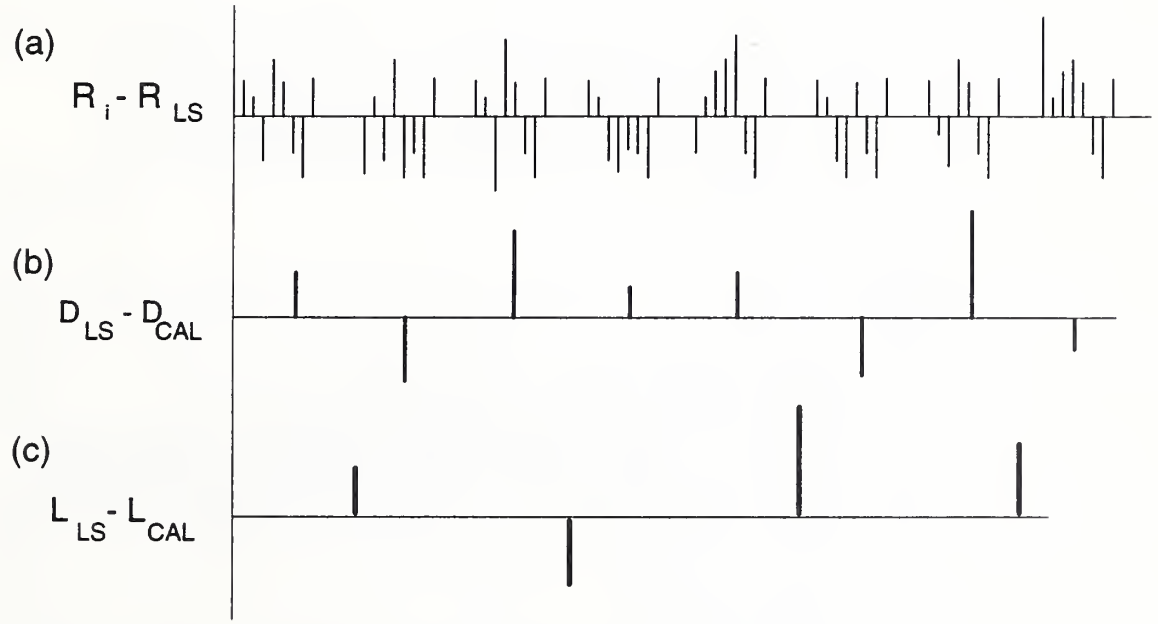

Figure 16 The results of an interim test, (a) deviations between the radii of each probing point and the best fit (least squares) radius, (b) deviations between the best fit sphere diameter and the calibrated diameter, (c) deviations between the center to center ball bar length and its calibrated length.

The design of a ball bar leads to a natural separation of CMM errors as described in Table 1. The variations in the probing point radii shown in Figure 14(a) identify short range CMM errors such

as probe lobing. This test is roughly equivalent to carrying out an abbreviated form of the ANSI point-to-point probe performance test at eight different positions within the CMM measuring volume. Since many points are taken on each sphere these short range errors, which are readily apparent in the radial deviation plot of Figure 14(a), tend to average out and not affect the results of the best fit sphere diameter or the center to center bar length. The sphere diameter values shown in Figure 16(b) test for incorrect effective stylus size, *e.g.* from an incorrectly calibrated reference sphere. This error is cleanly separated out and does not enter into either the radial deviation data, or the center to center bar length data. Finally the center to center bar length, shown in Figure 16(c), examines long range CMM errors and is largely independent of the errors detected in the other two plots. If this interim test had been carried out using a long gage block instead of a ball bar all of these errors would have been mixed together making it more difficult to identify the origin of the problem.

For purposes of regularly monitoring the interim test results, a summary chart can be easily constructed as shown in Figure 17. In this example we have plotted the largest measured radial deviation of each sphere, the sphere diameter deviations, and the bar lengths. The threshold limits and the testing frequency must be set by each user at an appropriate level for the particular CMM and the types of parts under measurement.

TABLE 1
Separation of CMM Errors in Ball Bar Measurements

Radial Deviations	• CMM Repeatability • Probe Repeatability • Probe Lobing • Stylus Ball Form • Stylus Bending • CMM Dynamics (Vibrations) • Probe Head Repeatability (using multiple head positions) • Probe Offset Vector Errors (using multiple styli or probe head positions) • Probe Changer Repeatability (using multiple probe changes per sphere) • Short Range Scale Errors
Ball Diameter	• Effective Stylus Diameter
Center to Center Ball Bar Length	• CMM Geometry (Squareness, Pitch, Roll, Yaw, etc.) • CMM Scale Temperature Compensation • Part Temperature Compensation

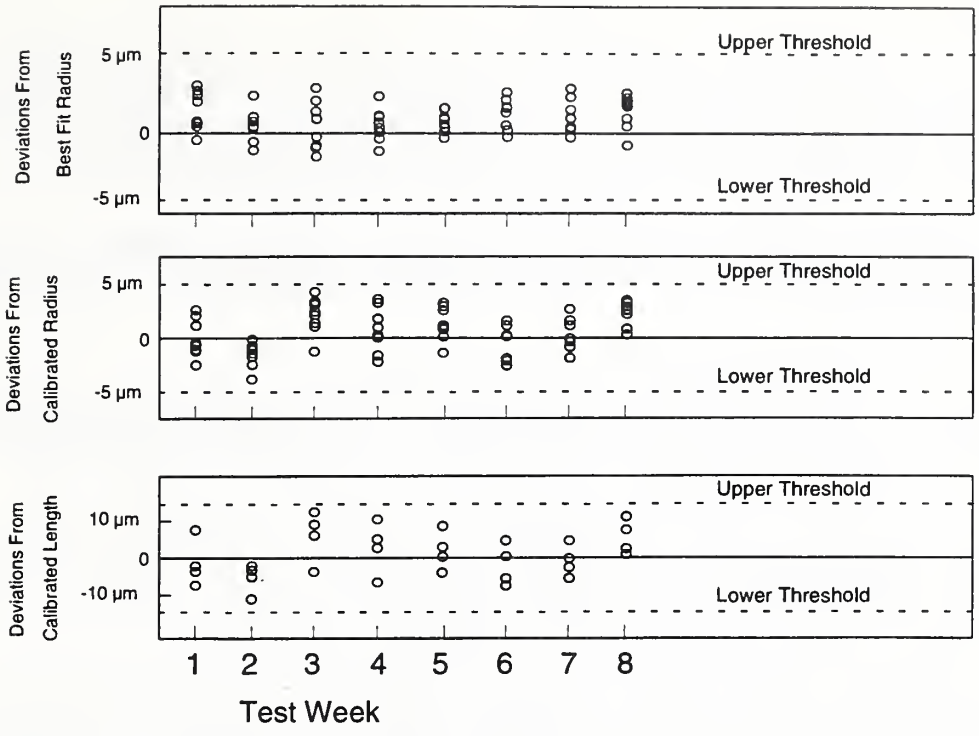

Figure 17 Interim test summary charts, (a) The largest radial deviation from each of the eight spheres measured, (b) the ball diameter deviations for all eight spheres, (c) the ball bar length deviations for all four positions. Threshold limits and testing frequency shown are for illustrative purposes only.

8 Summary

We have briefly reviewed the difficulties in dealing with measurement uncertainty relative to part tolerance. A discussion of using a gaging ratio rule and of specifying guard bands to protect the part tolerance from measurement uncertainty was presented. We have outlined the CIPM approach to uncertainty evaluation as it may apply to dimensional measurements. The simple case of determining the combined standard uncertainty remaining after a (first order) correction for a part's thermal expansion was presented in detail. We have examined many of the factors affecting CMM accuracy and emphasized the user's role in influencing potential CMM errors. Further work is needed both in determining the magnitudes of these errors (the variances) and their impact on the calculated result (sensitivity coefficients). This will involve developing new experimental methods of assessing CMM errors, and examining how specific combinations of sampling strategies and errors propagate through the fitting algorithm to influence the final result.

9 Acknowledgments

This research was partially funded by the US Air Force Calibration Coordination Group and the US Navy Manufacturing Technology Program. The authors wish to thank K. Eberhardt and J. Stone of NIST, and J. Bosch of Giddings & Lewis, for their comments.

10 References

1. D.A. Swyt, Challenges to NIST in Dimensional Metrology: The Impact of Tightening Tolerances in the U.S. Discrete-Part Manufacturing Industry, NISTIR 4757, National Institute of Standards and Technology, Gaithersburg MD 20899, Jan. 1992.

2. N. Taniguch, Current Status and Future Trends of Ultra precision Machining and Ultrafine Materials, Annals of the CIRP (International Institute of Production Research), Vol. 2 No 2, 1983

3. ISO, Guide to the Expression of Uncertainty in Measurement, prepared by ISO Technical Advisory Group 4(TAG4), Working Group 3, to be published (1993), International Organization for Standardization, Geneva Switzerland, draft version June 1992.

4. B.N. Taylor and C.E. Kuyatt, Guidelines for Evaluating and Expressing the Uncertainty of NIST Measurement Results, NIST Technical Note 1297, National Institute of Standards and Technology, Gaithersburg, MD 20899, Jan 1993.

5. NIST Technical Communications Program, Statements of Uncertainty Associated with Measurement Results, NIST Administrative Manual, Subchapter 4.09 Appendix E, National Institute of Standards and Technology, Gaithersburg, MD 20899, Jan 1993.

6. D.B. Dallas, "Dimensional Metrology, Tool and Manufacturing Engineers Handbook," Society of Manufacturing Engineers, Deaborn MI, 1976, p. 32-8.

7. U.S. MIL-STD-45662A, "Calibration System Requirements," U.S. Department of Defense, Washington DC 20301, 1988.

8. American National Standard, Dimensioning and Tolerancing, ANSI/ASME Y14.5 - 1982, The American Society of Mechanical Engineers NY NY, 1982.

9. U.S. MIL-HB-53B, "Evaluation of Contractor's Calibration System," U.S. Department of Defense, Washington DC 20301, 1989.

10. Private Communication with Mr. Frank Flynn, Newark AFB Ohio. Mr. Flynn is one to the authors of U.S. MIL-STD-45662A.

11. H.S. Nielsen, Uncertainty and Dimensional Tolerances, Quality, May 1993, p. 25-29.

12. R.G. Easterling, M.E. Johnson, T.R. Bement, and C.J. Nachtsheim, Absolute and Other Tolerances, SAND88-0724, LA-UR 88-906 (Sandia National Laboratories) 1989.

13. ANSI/ASME B89.1.12M 1985 and 1990 (revision 1), Methods for the Performance Evaluation of Coordinate Measuring Machines, sponsored and published by the American Society of Mechanical Engineers, United Engineering Center, 345 East 47th Street New York, NY 10017.

14 American National Standard, Temperature and Humidity Environment for Dimensional Measurement, ANSI B89.6.2 - 1979, The American Society of Mechanical Engineers NY NY, 1979.

15. VDI/VDE 2617 Accuracy of Coordinate Measuring Machines (1986), Beuth Verlag, D-1000 Berlin, Germany.

16. CMMA Accuracy Specification for Coordinate Measuring Machines (1989) London, England.

17. JIS B 7440 Test Code for Accuracy of Coordinate Measuring Machines (1987), Translated and Published by the Japanese Standards Association.

18. Mathematical Definition of Dimensioning and Tolerancing Principles, ASME Y14.5.1 Draft Standard, underdevelopment (1993).

19. A. Weckemnamm, M. Heinrichowski, and H.J. Mordhorst, Design of Gauges and Multipoint Measuring Systems using Coordinate Measuring Machine Data and Computer Simulation, Precision Engineering, **13**, 203-207 (1991).

20. C. Diaz, User's Guide for the Algorithm Testing System/Version 1.1, NISTIR 5137, National Institute of Standards and Technology, Gaithersburg MD 20899, Nov. 1992

21. Quality Assurance Program: Dimensional Inspection Techniques Specification (DITS) Proposal, CAM-I Arlington, Texas (1990.)

22. S.D. Phillips, B. Borchardt, W.T. Estler, and J. Henry, A Study on the Interaction of Form Error and Sampling Strategy for Spheres, to be published in the NIST Journal of Research.

Appendix A

Sources of Uncertainty in CMM Measurements

Probe properties	Comments
Effective stylus diameter (set by probe calibration)	Influenced by: probe calibration artifact size error, probe calibration artifact form error, calibration sampling strategy, probe type and stylus configuration, stylus bending, probe repeatability, probe lobing, probe approach speed, linearity or other geometry problems in analog probes, CMM repeatability, CMM dynamic behavior, variations in CMM geometrical errors over the calibration artifact. Effects non-unidirectional size measurements only.
Offset vector between different styli (set by multi styli calibration)	Influenced by probe type and stylus configuration, calibration sampling strategy, stylus bending, probe approach velocity, probe approach distance, probe repeatability, CMM repeatability, probe lobing, probe head repeatability (if applicable). Effects measurements which use multiple styli only.
Probe lobing (systematic directional dependent probe error)	Influenced by: probe type and stylus configuration (generally worse with longer stylus) stylus ball form error, probe approach speed. Effects can be reduced by averaging in some measurements, *e.g.* circles using many widely dispersed point; in some systems probe lobing is either absent or mapped out to the point where it is negligible compared to other considerations, *e.g.* probe repeatability.
Probe repeatability	Influenced by probe type and stylus configuration (generally worse with longer stylus) Effects can be reduced by averaging repeated measurements at each point.
Stylus bending	Influenced by stylus configuration, usually linear dependence on probing force, cubic dependence on stylus length, depends on stylus shaft material and shape, orientation of stylus to contact point, stylus mass, probe approach velocity. Effects can be reduced by using short stiff styli and low probing force
Indexable probe head repeatability	May be influenced by probe weight and stylus configuration. Effects measurements which use multiple probe head position positions only.
Stylus (or probe) changer repeatability	Effects measurements which interchange styli (or probes) only.
Probe spatial frequency response, and frictional effects	Influenced by inertial effects of probe, frictional effects (highly dependent on stylus ball - part interface), hardware and software filtering, probe velocity, probe dynamics. Effects primarily scanning probes, usually can be reduced by reducing probe velocity.

Sources of Uncertainty in CMM Measurements (continued)

CMM properties	Comments
errors in rigid body geometry (at standard temperature)	18 position dependent functions, 3 scalar variables (squareness) uncertainties are ellipsoids whose size, aspect ratio, and orientation may be highly location dependent in the machine coordinate system. If CMM is error mapped the residual uncertainties are dependent on error map coordinate system. Influenced by direction of motion, number or servos active, and probe offset vector.
Non-rigid body geometry errors (quasi static conditions)	Uncertainties are ellipsoids whose size, aspect ratio, and orientation may be highly location dependent in the machine coordinate system, and if the CMM is error mapped, dependent on the location of the error map coordinate system. May depend on direction of motion, number or servos active, and probe offset vector.
CMM part loading effects	CMM errors usually increases with increasing part load, depends on magnitude and distribution of load on CMM table.
CMM dynamic behavior	Position uncertainty usually increases if the CMM is in motion when recording data due to structural deformations arising from inertial effects and vibrations. Depends on velocity, acceleration, number of servos active, CMM supporting structure. Effects can be usually be reduced by increasing probe approach distance, decreasing probe speed and acceleration.
CMM repeatability	Repeatability may be direction dependent (hysteresis) and location (in the CMM workzone) dependent, usually worst when the ram is fully extended and with large probe offsets. Includes effects of scale resolution
Algorithm accuracy	Some algorithms include calculational simplifications which can lead to inaccuracies.
Thermally induced errors in a uniform and constant, but non-standard temperature environment	Uncertainties include the expansion of CMM scales, if uncorrected the total expansion, if corrected the uncertainty in the expansion coefficient and temperature measurement. If the CMM is made of materials with different thermal expansion coefficients then geometrical distortions of the CMM structure (and possibly the scales) may result.
Thermally induced errors in a non-constant temperature environment	Geometrical errors depend on the temperature distribution of machine structure at every point; infinite number of possible combinations. Large spatial gradients in machine structure can produce large errors. Note spatial gradients can be induced even in a homogeneous temperature environment if it is varying with time due to the different thermal time constants of components in the CMM. It may be possible to place upper limits on the errors by specifying combinations of environmental conditions, e.g. spatial gradients (°C/m), temporal gradients (°C/hr) temperature range (± °C). Thermal mapping techniques may reduce some errors.
Other environmental factors	Atmospheric pressure, humidity, and composition can affect interferometrically based scales. Humidity may effect the geometry of some materials.
Variations in utility services: air pressure, electrical power, water supply.	Many CMMs require external utility services, variations in air pressure to air bearings may induce geometry, and repeatability errors, air temperature can cause thermal errors, electrical power fluctuations may cause problems with electronics, cooling water pressure or temperature variations, may cause thermal errors.

Sources of Uncertainty in CMM Measurements (continued)

Part properties	Comments
Part dynamics	Part bending under probing force, part vibration (CMM velocity and acceleration dependent). Stylus force may penetrate into part material, depends on stylus-part materials and geometry.
Part fixturing	distortion due to clamping; slippage under probing force; thermally induced distortion due to over constrained clamping; improper mounting per part function; distortions due do part weight
Part thermal properties	uniform expansion: uncertainties in part temperature measurement and thermal expansion coefficient, non-uniform part temperature; part distortion due to non-uniform part temperature or different materials.
User selected properties	Comments
CMM operating parameters	Selection of probe approach speed, probe approach direction, acceleration parameters, all effect the resultant error introduced by the CMM and probe
Algorithm Selection	Data analysis algorithm may produce a substitute geometry which is not equivalent to the geometry required for part function.
Sampling strategy (incomplete part geometry information)	Selection of number and location of sampling points on part surface determines what information is used in the fitting algorithm; sampling strategy also determines some CMM errors (direction of probe approach effects CMM dynamics, repeatability, lobing, probe repeatability, etc.). Poor sampling strategy selection can produce significant errors in computed results due to incomplete information on part geometry. Some sampling strategies are unstable.
Part location and orientation	Part location can effect CMM errors